Superconductor Science and Technology

# Magneto-transport studies of $FeSe_{0.9-x}M_x$ (M = Si, Sb)

To cite this article: Swati Pandya *et al* 2011 *Supercond. Sci. Technol.* **24** 045011

Supercond. Sci. Technol. **24** (2011) 045011 (8pp) doi:10.1088/0953-2048/24/4/045011

# Magneto-transport studies of $FeSe_{0.9-x}M_x$ (M = Si, Sb)

**Swati Pandya[1], Siya Sherif[1,2], L S Sharath Chandra[1,3] and V Ganesan[1,4]**

[1] UGC-DAE Consortium for Scientific Research, University Campus, Khandwa Road, Indore (MP) 452017, India
[2] Department of Studies in Physics, University of Mysore, Manasagangothri, Mysore 570 006, India

E-mail: vganesancsr@gmail.com

Received 14 October 2010, in final form 18 January 2011
Published 10 February 2011
Online at stacks.iop.org/SUST/24/045011

**Abstract**

We report on the magneto-resistivity of $FeSe_{0.9-x}M_x$ (M = Si, Sb, $x = 0.05, 0.1$) down to 2 K in the presence of magnetic fields up to 14 T. The superconducting transition shows marginal differences for Sb-and Si-doped samples. Normal state resistivity shows marked changes at intermediate temperatures around 100 K, signaling the presence of a structural transition. It also shows linear behavior with temperature, reminiscent of high $T_c$ ceramics. Superconducting parameters like critical fields and coherence lengths are quantified for all samples. The broadening of superconducting transitions is studied through thermally activated flux flow (TAFF) and fluctuation conductivity. The activation energy of these superconductors is found to be one order smaller than the FeAs-1111 system, which may be explained in terms of larger penetration depth. The activation energy of thermally activated flux flow decreases with the Si and Sb doping and is explained by Kramer's scaling for grain boundary pinning. The zero-field and magnetic-field-induced fluctuation conductivity are studied using Aslamazov–Larkin (AL) and lowest Landau level (LLL) theories, respectively. Zero-field fluctuation conductivity shows the 2D to 3D crossover just above the mean-field transition and 3D LLL scaling is obtained near mean-field transitions for magnetic-field-induced fluctuation conductivity. This is a clear indication of the three-dimensional nature of these superconductors. The 3D nature of these superconductors signifies its potential for future technological applications.

(Some figures in this article are in colour only in the electronic version)

## 1. Introductions

Superconductivity in the class of new Fe-based materials is known to be unconventional, with electron pairing possibly mediated by magnetic interactions [1]. This makes these systems more interesting. Superconductivity was recently reported for Fe-based chalcogenides, which are very similar to that of the Fe–As based superconductors [2]. In chalcogenide systems, the superconductivity was first reported in polycrystalline FeSe at 8 K, followed by pressure studies that indicated a superconducting onset temperature near 27 K for the modest pressure of 15 kbar [2]. Recently Medvedev *et al* have given the magnetic and electronic phase diagram of FeSe as a function of temperature and pressure and showed that the superconductivity transition increases up to 36.7 K under an applied pressure of 8.9 GPa [1]. Te substitution in the $FeSe_{1-x}Te_x$ system enhances the $T_c$ in spite of negative chemical pressure [3–6]. Apart from the superconducting transition, FeSe shows a tetragonal to orthorhombic structural transition around ∼100 K [1, 7–9]. Therefore it is interesting to study the effect of positive and negative chemical pressure on the superconducting and structural transition in the FeSe system. With the aim of studying negative and positive chemical pressure effects, we have substituted Si and Sb at the site of Se for the $FeSe_{0.9}$ system, where Si has a smaller and Sb has a bigger ionic radius as compared to Se. In addition to this, Si substitution adds two holes while Sb substitution

[3] Present address: Materials, Advanced Accelerator Science Division, Raja Ramanna Centre for Advanced Technology, Indore 452 013, India.
[4] Author to whom any correspondence should be addressed.

 

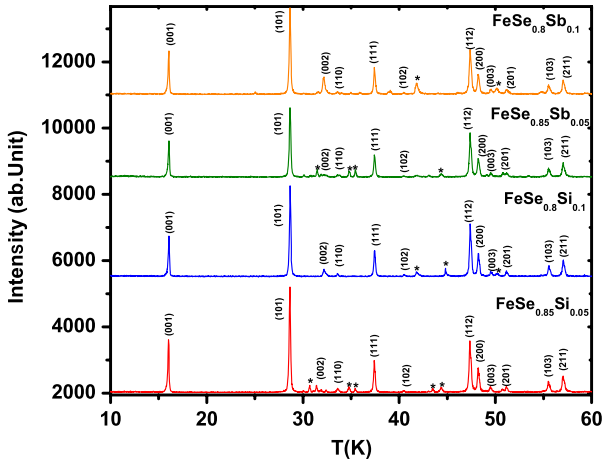


**Figure 1.** X-ray diffraction of $FeSe_{0.9-x}M_x$ (M = Si, Sb, $x = 0.05, 0.1$). The peak with (∗) symbol indicates impurity phase.

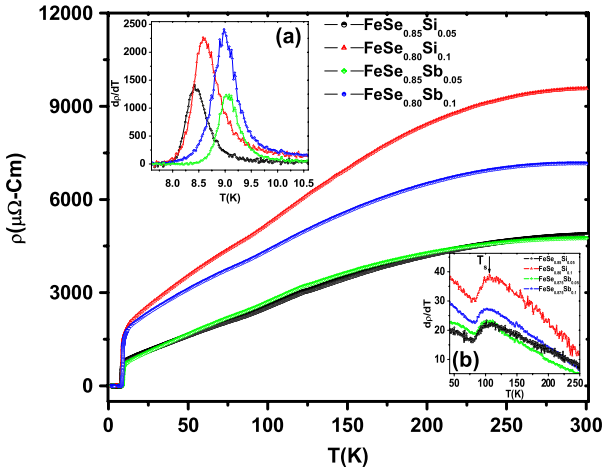


**Figure 2.** Zero-field resistivity for $FeSe_{0.9-x}M_x$ (M = Si, Sb, $x = 0.05, 0.1$) in temperature range 2–300 K. Insets show (a) derivative of resistivity near superconducting transition for all four samples and (b) derivative of resistivity near structural transition for $FeSe_{0.9-x}M_x$ (M = Si, Sb, $x = 0.05, 0.1$).

adds one hole to the system, which is another interesting aspect to study the effect of hole substitutions in the $FeSe_{0.9}$ system. Recently Ge *et al* have reported a preliminary study on transport properties of $Fe(Se_{1-x}Sb_x)_{0.92}$ [9].

In this paper, we present the magneto-transport studies of the hole-doped $FeSe_{0.9-x}M_x$ (M = Si, Sb) ($x = 0.05, 0.1$) system. The effect of Si and Sb doping on the superconducting transition and structural transition are studied. Critical field and coherence lengths are calculated for all the samples. The broadening of the superconducting transition is studied through thermally activated flux flow and fluctuation conductivity. Recently, Ge *et al* have observed the 3D nature of fluctuations in the FeSe system for zero-field fluctuation conductivity [10]. Here we have studied magnetic-field-induced fluctuation conductivity in addition to zero-field fluctuation conductivity for a detailed dimensionality investigation, as dimensionality is one of the important aspects which decides the potential of a system for applications. The zero-field and magnetic-field-induced fluctuation conductivity of the superconductor are analyzed using Aslamazov–Larkin (AL) theory and lowest Landau level (LLL) scaling, respectively.

## 2. Experimental details

Polycrystalline samples $FeSe_{0.9-x}M_x$ (M = Si, Sb) ($x = 0.05, 0.1$) are prepared using the solid state reaction method. The constituents were weighed and sealed in a quartz tube in the presence of helium gas and annealed at 600 °C for one day. After that, the obtained mixture was ground into a fine powder and made into pellet form. The pellet was sealed in a quartz tube in the presence of helium and annealed at 700 °C for one day. The sample was reground and made into pellet form and sealed in a quartz tube in the presence of helium followed by a third annealing at 700 °C for two days and then slowly cooled down to 400 °C. The samples were kept at 400 °C for three days and then quenched to liquid nitrogen temperature. The samples were characterized by x-ray diffraction using Cu K$\alpha$ radiation in a Rigaku diffractometer. The resistivity is measured down to 2 K in a magnetic field up to 14 T with a conventional four-probe method using a Quantum Design physical property measurement system.

## 3. Results and discussions

X-ray diffraction patterns for $FeSe_{0.9-x}M_x$ (M = Si, Sb, $x = 0.05, 0.1$) are shown in figure 1. These patterns indicates that the samples are formed in tetragonal $P4/nmm$ structure with a small amount of hexagonal FeSe and $Fe_7Se_8$ impurity phase, which is generally found in the preparation of FeSe [2, 3, 5, 8–15]. The lattice parameters estimated from Rietveld refinements indicate that there is no noticeable change in lattice parameters with Si doping while that for Sb doping increases slightly. This is attributed to the ionic radius of Se, which is almost the same as that of Si, while the ionic radius of Sb is markedly larger than Se. However, Ge *et al* have not found any systematic change of lattice parameters for $Fe(Se_{1-x}Sb_x)_{0.92}$ ($x = 0, 0.05, 0.1, 0.2$) [9].

The zero-field resistivity of $FeSe_{0.9-x}M_x$ (M = Si, Sb, $x = 0.05, 0.1$) shows onsets of superconductivity at 9.7 K, 10.4 K, 10.3 K and 10.7 K, respectively, as shown in figure 2. Normal state resistivity shows metallic behavior at low temperatures and saturation-like behavior near room temperature which is attributed to the metal–insulator transition above room temperature [9]. Inset (a) of figure 2 shows the derivative of resistivity neat $T_c$ for all four samples. Even though marginal, derivatives of resistivity show that the Sb-doped samples have a higher superconducting transition temperature than the Si-doped samples. The mean-field $T_c$ obtained from the derivative of resistivity are 8.4 K, 8.6 K, 9.1 K and 9 K for 5% Si, 10% Si, 5% Sb and 10% Sb samples, respectively. This is in agreement with the mean-field $T_c$ for $Fe(Se_{1-x}Sb_x)_{0.9}$ ($x = 0.05, 0.1$) that is reported in the literature [9]. The broadening of the superconducting transition as well as the normal state resistivity increases with increasing Si and Sb doping. It is observed in the literature that the substitution of sulfur (S) and manganese (Mn) at

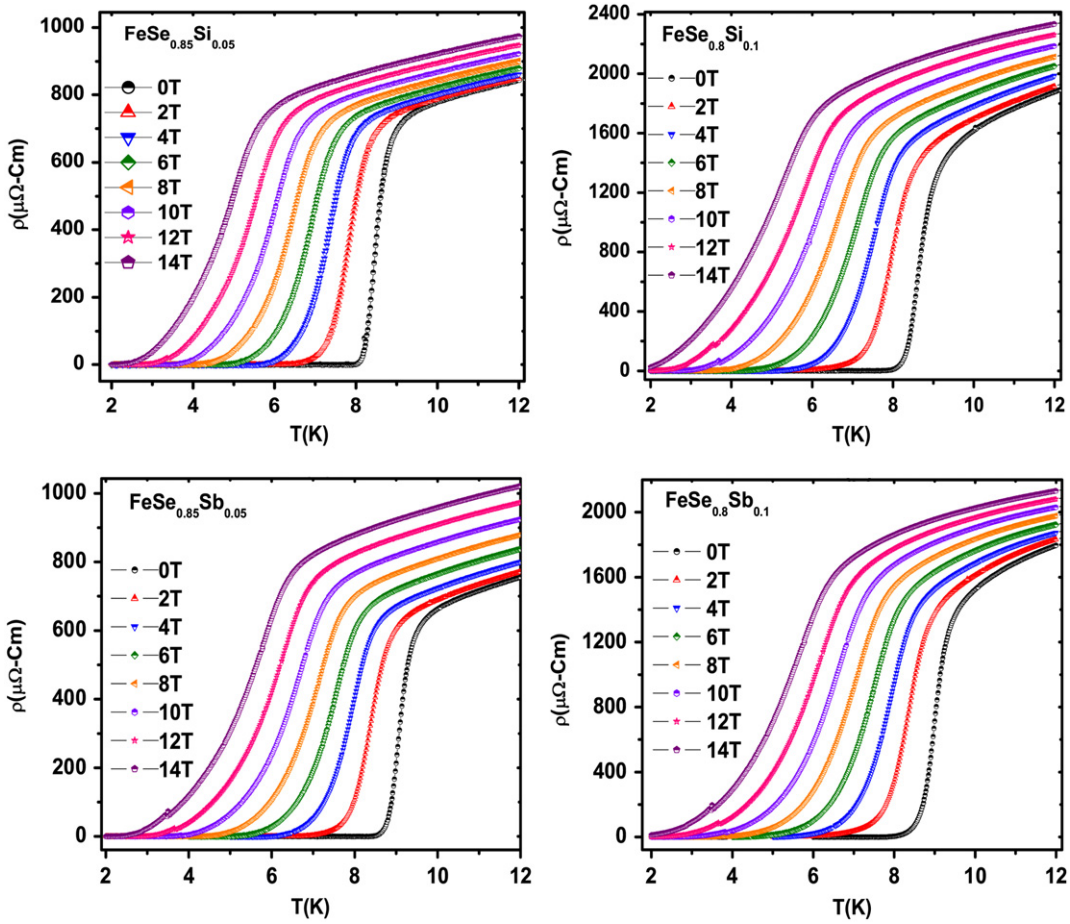


**Figure 3.** Resistivity of $FeSe_{0.9-x}M_x$ (M = Si, Sb, $x = 0.05, 0.1$) near superconducting transition down to 2 K and in magnetic field up to 14 T.

the site of Se in FeSe increases the resistance of the system along with a slight increase in the superconducting transition temperature [6, 14, 16]. As we have shown in inset (a) of the figure 2, Si doping shows a slight increase in mean field and onset transition but no change in $T_c$ zero whereas Sb doping shows almost the same onset with decrease in mean-field $T_c$ and $T_c$ zero. These observations indicate that the broadening of the superconducting transition is due to doping-induced disorder for Sb-doped samples, while more investigations are needed to understand the slight increase in mean field and onset transitions in Si-doped samples.

The resistivity shows a slope change around ∼100 K for all the samples, which is associated with the tetragonal to orthorhombic structural transition [1, 7–9]. The accurate structural transitions are obtained from the hump behavior in the derivative of resistivity as shown in inset (b) of figure 2. The structural transition temperatures are at 108 K, 112 K, 106 K and 104 K for 5% Si-, 10% Si-, 5% Sb-and 10% Sb-doped samples, respectively. The structural transition temperature is slightly shifted towards the higher temperature side with Si doping and towards the lower temperature side with Sb doping. The observed behavior is in agreement with that for $Fe(Se_{1-x}Sb_x)_{0.92}$ and $FeSe_{1-x}S_x$ [9, 14]. Figure 3 shows the resistivity for all the samples down to 2 K and in the presence of a magnetic field up to 14 T. The superconducting

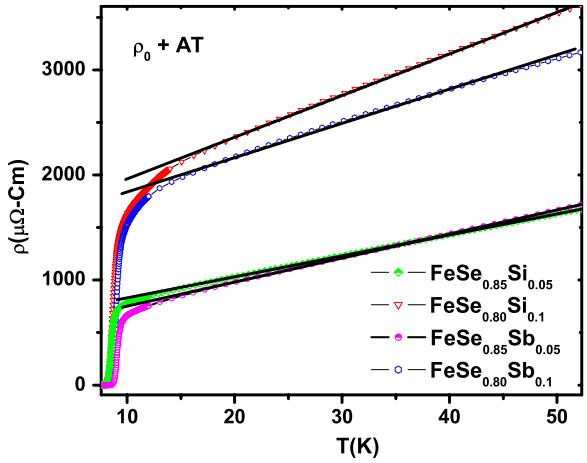


**Figure 4.** Zero-field resistivity of $FeSe_{0.9-x}M_x$ (M = Si, Sb, $x = 0.05, 0.1$) in temperature range 12–50 K with least-squares fit to the equation $\rho_0 + AT$.

transitions broaden further with application of a magnetic field. The onset of the superconducting transition is effectively shifting towards the lower temperature side with increase in the magnetic field. However, no noticeable field effect is seen in normal state resistivity.

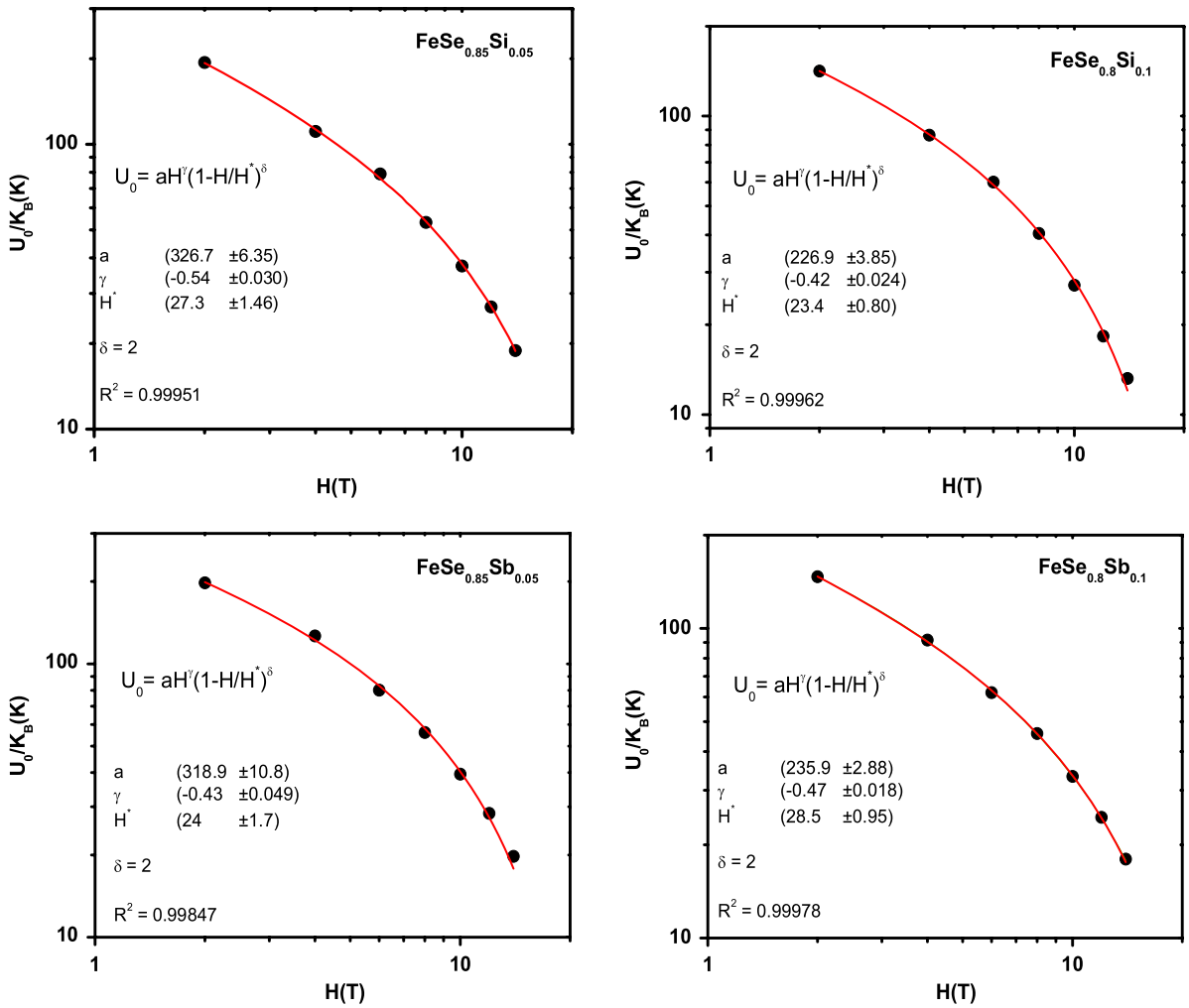


**Figure 5.** Activation energy ($U_0/K_B$) of thermally activated flux flow versus magnetic field for $Fe(Se_{1-x}M_x)_{0.9}$ (M = Si, Sb, $x = 0.05, 0.1$) with Kramer's model fit with fitting parameters.

As shown in figure 4, the normal state resistivity shows $\rho_0 + AT$ behavior below the structural transition for all the samples. This is in contradiction to the $T^2$ behavior of the Fermi liquid state as observed for the 1111-FeAs family [17]. This linear temperature dependence of resistivity is a characteristic of high $T_c$ ceramics and is attributed to the non-Fermi liquid-like behavior [8, 9]. The linear temperature dependence of resistivity in FeSe is ascribed to the antiferromagnetic fluctuations or short range magnetic order [9].

The critical field ($H_{c2}$) is obtained from the linear extrapolation of $H$ versus $T_c$ plot and using the Werthamer–Helfand–Hohenberg (WHH) theory [17, 18], where $H_{c2}^{WHH}(0)$ is given by $0.693T_C(dH_{c2}/dT)_{T_c}$, where $T_c$ is the mean-field superconducting transition. The $H_{c2}$ estimated from linear extrapolation and from WHH theory are 35 T, 38 T and 25 T, 26 T respectively for 5% Si-and 10% Si-doped $FeSe_{0.9}$. An uncertainty in estimation of the upper critical field from linear extrapolation and WHH theory depends upon the estimation of mean-field $T_c$ as well as upon the linear fit for $H$ versus $T_c$ plot. The mean-field $T_c$ is taken from the derivative of resistivity, where resistivity near the superconducting transition is measured with an interval of 0.02 K. The errors in the linear fits for extrapolated critical field to get the slope $dH_{c2}/dT$ to estimate the upper critical field are less than 2%. The coherence length estimated using Ginzburg–Landau theory, i.e. $\xi^2 = \varphi_0/2\pi H_{c2}$, ($\varphi_0$ is the magnetic flux quantum) by taking the estimated values of $H_{c2}$ are 30.6 Å, 29.5 Å, and 36.6 Å, 35.3 Å for 5% Si and 10% Si, respectively. The errors in the estimation of $\xi$ are of the same magnitude as that of $H_{c2}$ as $\xi$ is determined solely by $H_{c2}$. The critical field values of 40 and 39 T from linear extrapolation and 28 and 27 T from WHH theory, estimated for 5% Sb and 10% Sb samples, are slightly higher as compared to Si-doped samples. Hence, the coherence lengths are estimated to be about 28.8 Å, 29.2 Å, and 34.3 Å, 34.9 Å respectively for 5% Sb and 10% Sb samples.

The broadening of the superconducting transition in the presence of a magnetic field is studied through thermally activated flux flow (TAFF) [17, 18]. The activation energy of flux flow in different magnetic fields is obtained from the Arrhenius law: $\rho(T, H) = \rho_0 \exp[-U_0/K_B T]$, where $U_0$ is the activation energy of TAFF, $K_B$ is the Boltzmann constant and $\rho_0$ is the pre-exponential factor [17, 18]. The activation energy versus magnetic field is plotted in figure 5 for all the

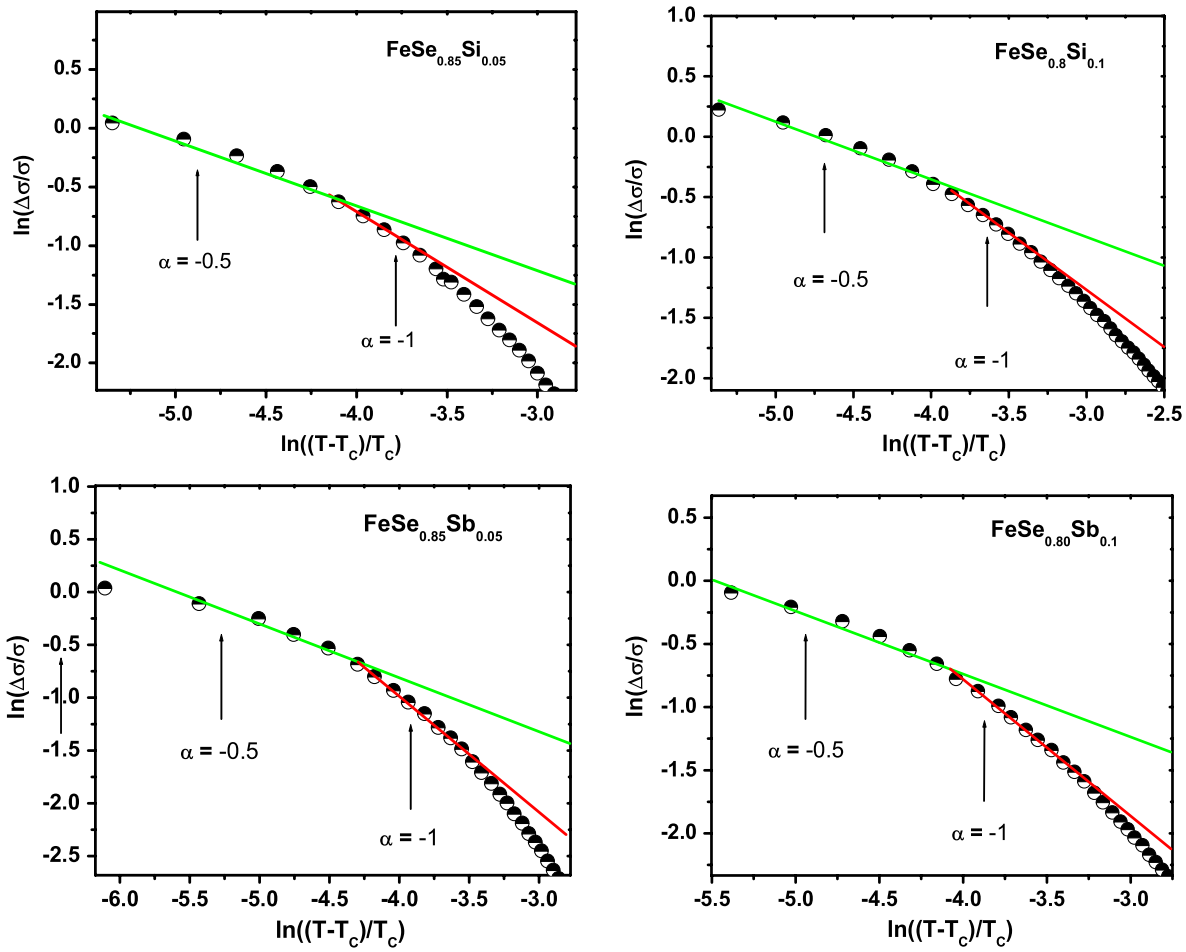


**Figure 6.** ln–ln plot of excess conductivity ($\Delta\sigma/\sigma$) near superconducting transition versus reduced temperature $(T - T_c)/T_c$ for $FeSe_{0.9-x}M_x$ (M = Si, Sb, $x = 0.05, 0.1$).

samples. The obtained $U_0/K_B$ for a low field 2 T is 194 K, 142 K, 198 K and 147 K for 5% Si, 10% Si, 5% Sb and 10% Sb samples, respectively. The $U_0/K_B$ decreases with increase in Si and Sb doping. The value of $U_0/K_B$ is slightly higher for Si-doped samples as compared to Sb-doped samples. The activation energy of these samples at low fields is of the same order as for the $NbSe_2$ and $FeTe_{1-x}S_x$ systems [18, 19], while almost one order smaller than the FeAs (1111), $MgB_2$ and high $T_C$ cuprate superconductors [17, 19, 20]. The magnitude of activation energy at low magnetic field is given by $U_0 \sim \varphi_0^2\xi/48\pi^2\lambda^2$ and experimental results are in good agreement with this calculation [19, 21]. This relation indicates that the magnitude of $U_0$ strongly depends on coherence length ($\xi$) and penetration depth ($\lambda^2$) as it is proportional to $\sim\xi/\lambda^2$. If we compare the FeSe system with to FeAs-1111 system, then there is not much difference between coherence lengths of these superconductors but there is a large difference in penetration depths reported. For instance, penetration depth of FeAs-1111 superconductors is about 200 nm [22–24], while for FeSe it is about 405 nm [25], which is almost double. This may be a reason for the one order smaller activation energy of the $FeSe_{0.9-x}M_x$ (M = Si, Sb, $x = 0.05, 0.1$) system as compared to the FeAs-1111 systems. Scaling for log $\rho(T, H)$ versus $U_0$ $(1/T–1/T_m)$ plots is not seen in these samples, as observed for $FeTe_{1-x}S_x$ and FeAs-1111 superconductors [17, 18]. Magnetic field dependence of the activation energy shows parabolic behavior instead of power-law behavior observed for $FeTe_{1-x}S_x$, FeAs-1111 and high $T_C$ cuprates [17–20, 26, 27].

It is to be noted that our earlier studies on $FeTe_{1-x}S_x$ [18] show the same onset of superconducting transition for zero field and high magnetic field, while there is a noticeable change in the onset of superconducting transition for the present samples. This observation indicates that a different pinning mechanism is involved for both systems even though both systems are from the same 11-family with similar crystal structure.

The vortex activation energy can be explained by the following equation [19, 21]:

$$U_0(B) = aB^{\gamma}(1 - B/B^*)^{\delta} \quad (1)$$

where $B$ is the applied magnetic field, $B^*$ is the irreversibility field or simply the upper critical field and $a$, $\gamma$ and $\delta$ are scaling parameters. The $B^{\gamma}$ and $(1 - B/B^*)^{\delta}$ terms of this relation are related to critical current density variation and suppression superconducting properties with the application of a field. This relation is well fitted for magnetic field dependence of activation energy. The $U_0/K_B$, along with the fitting and

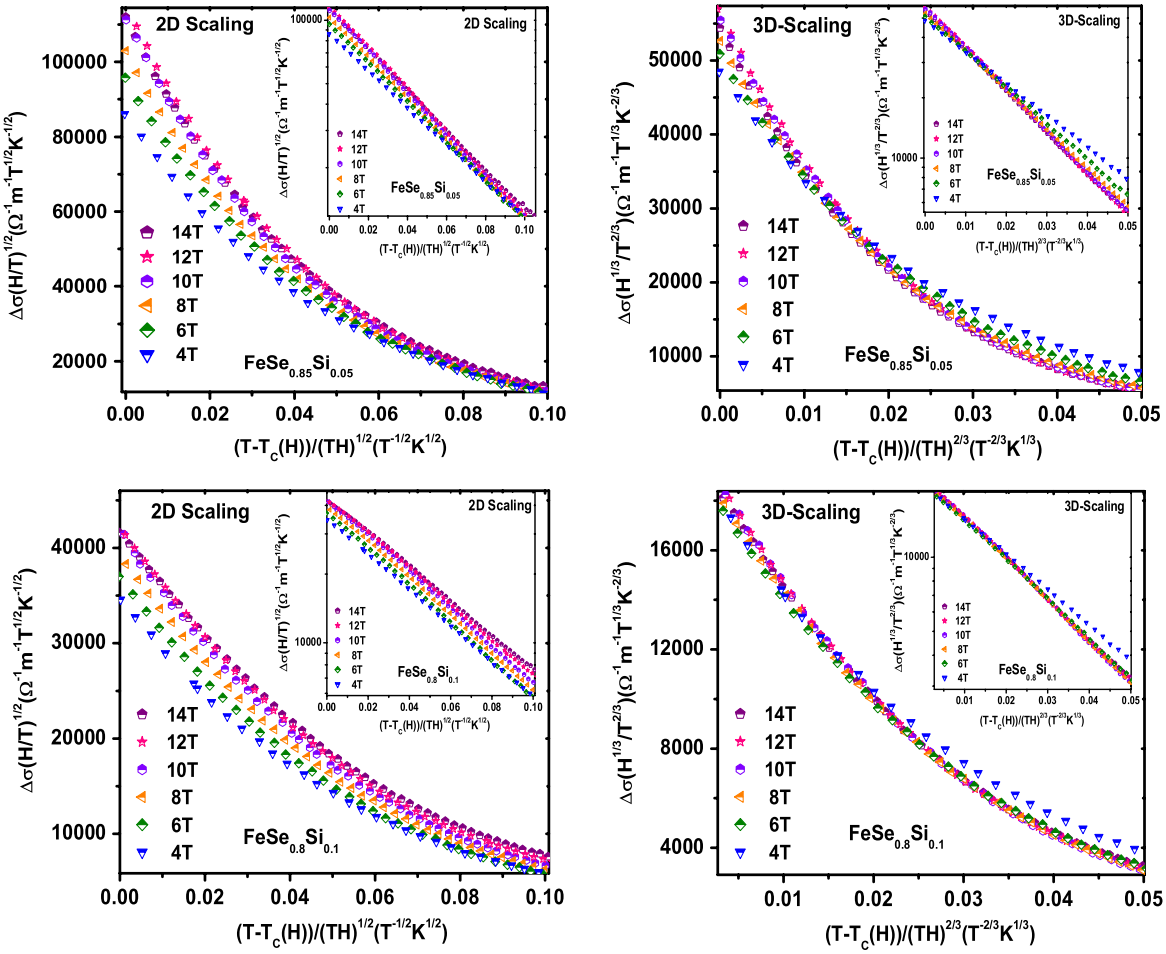


**Figure 7.** 2D and 3D LLL scaling for $FeSe_{0.9-x}Si_x$ ($x = 0.05, 0.1$) up to 14 T. Insets show same plots in semi-logarithmic scale.

fitting parameters for all the samples, are shown in figure 5. The $\delta$ is fixed as 2, $\gamma$ is found to be $-0.4$ to $-0.5$ and $B^*$ is roughly the same as the upper critical field ($H_{c2}$) obtained from the WHH theory. These fitting parameters indicate that the activation energy can be explained by Kramer's scaling law for flux pinning force density, i.e. $F_P \propto (B/B^*)^{1/2}(1 - B/B^*)^2$ [19, 21]. Similar behavior is observed for $MgB_2$ and $NbSe_2$ superconductors [19, 21], where the parabolic dependence is interpreted as a consequence of strong grain boundary pinning.

The broadening of the superconducting transition is further analyzed using fluctuation conductivity [18]. To study the zero-field fluctuation conductivity, excess conductivity ($\Delta\sigma/\sigma$) versus temperature is plotted as shown in figure 6. The zero fluctuation conductivity is studied through a 2D and 3D Aslamazov–Larkin (AL) model [18, 28, 29]. Aslamazov–Larking theory predicts that

$$\Delta\sigma/\sigma_0 = At^{\alpha} \tag{2}$$

where $\sigma_0$ is the conductivity extrapolated from the normal conductivity, $T_c$ is the mean-field superconducting transition, $t$ is the reduced temperature $(T - T_c/T_c)$, $A$ is the temperature-independent amplitude and $\alpha$ is the conductivity exponent, which should be $-0.5$ for the three-dimensional and $-1$ for the two-dimensional nature of fluctuations [18, 28, 29]. The conductivity exponent is estimated by fitting a straight line for $\ln(\Delta\sigma/\sigma)$ versus $\ln(T - T_c/T_c)$. The error associated with the conductivity exponent from this linear fit varies from 6% to 7% for all these samples. Conductivity exponents indicate crossover from 2D to 3D above the mean-field transitions for all samples as shown in figure 6. The 2D to 3D crossover temperatures are 8.6 K, 8.8 K, 9.2 K and 9.1 K for 5% Si, 10% Si, 5% Sb and 10% Sb samples, respectively. However, due to the limited range of reduced temperature over which such a crossover is seen, we have added further analysis of resistive broadening in the presence of a magnetic field to confirm the 3D nature of the results.

In the presence of strong magnetic fields, quasiparticles are confined to the lowest Landau level and transport becomes one-dimensional along the direction of applied field and hence the fluctuation effects near $T_c$ increase due to low effective dimensionality of the system [18, 24]. The temperature range for fluctuation conductivity near $T_c$ enhances in the presence of magnetic field, where one can study the dimensionality of a system more precisely. We have applied lowest Landau level (LLL) scaling to study the magnetic-field-dependent fluctuation conductivity of these samples as reported for the $FeTe_{1-x}S_x$ system [18]. There exists a scaling law for excess

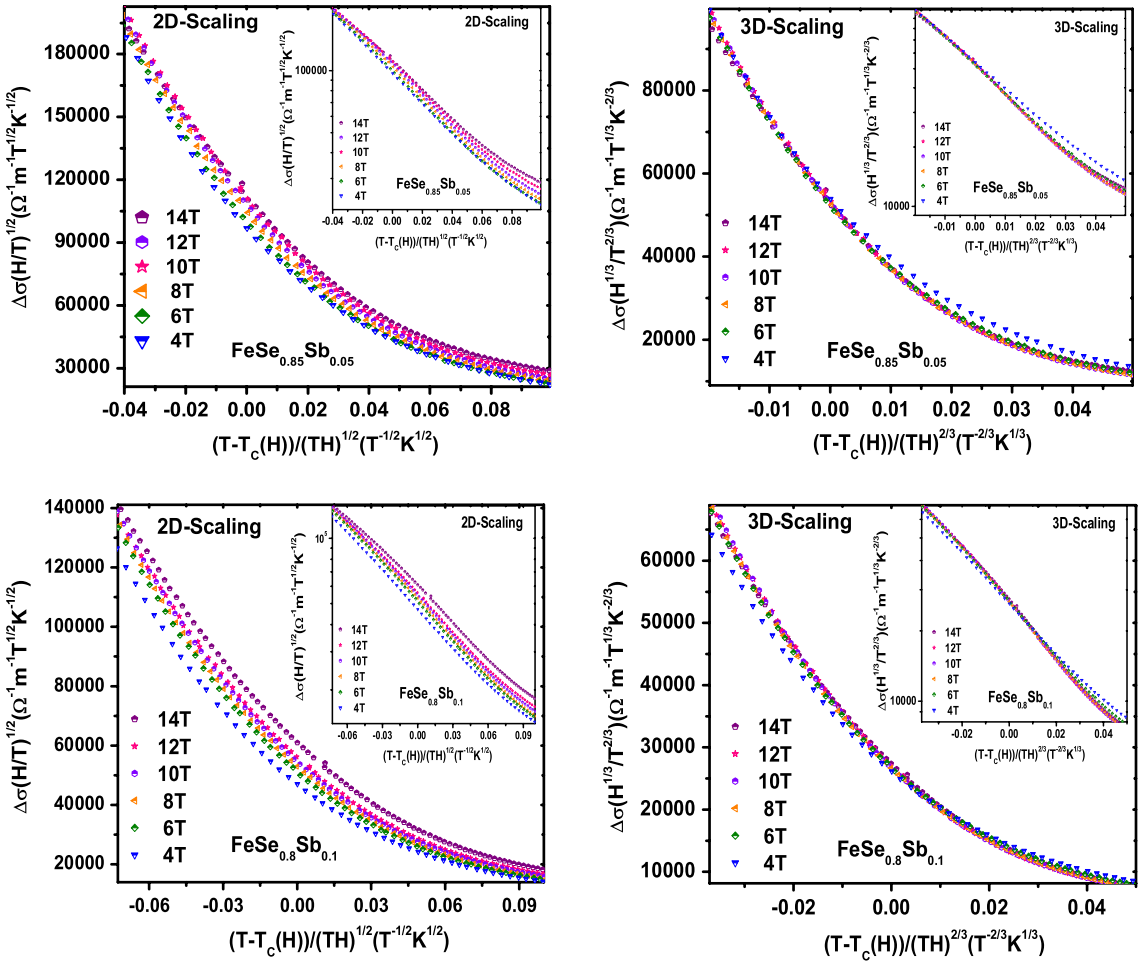


**Figure 8.** 2D and 3D LLL scaling for $FeSe_{0.9-x}Sb_x$ ($x = 0.05, 0.1$) up to 14 T. Insets show same plots in semi-logarithmic scale.

conductivity ($\Delta\sigma$) due to fluctuations in magnetic fields in terms of unspecified scaling functions $F_{2D}$ and $F_{3D}$, valid for 2D and 3D cases, respectively:

$$\Delta\sigma(H)_{2D} = (T/H)^{1/2} F_{2D}(A[(T - T_c(H))/(TH)^{1/2}]) \quad (3)$$

$$\Delta\sigma(H)_{3D} = (T^2/H)^{1/3} F_{3D}(B[(T - T_c(H))/(TH)^{2/3}]) \quad (4)$$

where $A$ and $B$ are characteristic constants of the material. Assuming the Landau level spacing is larger than the Landau level interaction energy, there exists a field $H_{LLL}$ above which the LLL approximation should hold [18, 24, 30–32]. Such a scaling has been reported to be successful in the high $T_c$ cuprates, new 1111-FeAs and $FeTe_{1-x}S_x$ superconductors [18, 24, 30–32]. Figures 7 and 8 show 2D and 3D LLL scaling for Si-and Sb-doped samples, respectively. Insets show the same plots in a semi-logarithmic scale. The temperature range is the same for 2D and 3D scaling. The free parameter used for LLL scaling is the mean-field $T_c(H)$ at different magnetic fields. Here $T_c(H)$ is determined by optimizing the scaling fit. The uncertainty in mean-field $T_c$ estimated from scaling and that from experiments is less than 1%. It is clearly visible that the 3D scaling is better as compared to the 2D scaling for all the samples. The 3D scaling for magnetic-field-induced fluctuation conductivity is observed below the crossover temperature of 2D to 3D zero-field fluctuations for all samples. The 3D scaling is observed above $H_{LLL} \sim 6$ T for $FeSe_{0.85}Si_{0.05}$ and above $H_{LLL} \sim 4$ T for the remaining three samples.

Detailed dimensionality studies have been done for $SmFeAsO_{1-x}F_x$ [24] and $FeTe_{1-x}S_x$ [18] superconductors among all the new Fe-based superconductors, where both systems are proven to be two-dimensional in nature, whereas zero-field and magnetic-field-dependent fluctuation conductivity studies of $FeSe_{0.9-x}M_x$ (M = Si, Sb, $x = 0.05, 0.1$) indicate that the nature of superconducting fluctuations is three-dimensional for these superconductors. The three-dimensionality of $FeSe_{0.9-x}M_x$ (M = Si, Sb, $x = 0.05, 0.1$) superconductors signifies its potential for future technological applications. FeSe systems have smaller interlayer distance (~5.5 Å) as compared to FeAS-1111(~8 Å) and $FeTe_{1-x}S_x$ (~6.2 Å) systems, which leads to the 3D nature of the superconductor. However, there is a good possibility for the FeTe-derived system to be a 3D superconductor with proper tuning of chemical substitution, as FeTe and FeSe systems have smaller differences in lattice parameters along the $c$ axis. Hence, it will be interesting to study the dimensionality in the Fe(Se, Te) system.

## 4. Conclusion

The hole substitution through Si and Sb doping for the $FeSe_{0.9}$ system slightly increases the superconducting transition temperature and makes the transition broaden. However, Sb-doped samples have higher $T_c$ than the Si-doped samples. The tetragonal to orthorhombic structural transition is observed around ∼100 K, which is slightly shifted towards the higher temperature side with Si doping and towards the lower temperature side with Sb doping. The normal state resistivity below the structural transition shows non-Fermi liquid behavior for all four samples. The obtained critical field values obtained using WHH theory are ∼25–28 T and calculated coherence length is around ∼30 Å for these systems. The activation energy ($U_0/K_B$) for thermally activated flux flow decreases with Si and Sb doping. Activation energy is slightly higher for Si-doped samples as compared to Sb-doped samples. Magnetic-field-dependent $U_0/K_B$ shows a parabolic behavior, which is explained by Kramer's scaling for grain boundary pinning. The zero-field fluctuation conductivity shows the 2D to 3D crossing just above the mean-field transition, which is further supported by 3D LLL scaling near the mean-field transition above $H_{LLL} \sim 6$ T for $FeSe_{0.85}Si_{0.05}$ and above $H_{LLL} \sim 4$ T for the remaining three samples. The magnetic-field-dependent fluctuation conductivity proves the three-dimensional nature of these superconductors. The three-dimensionality of these superconductors signifies their potential for future technological applications.

## Acknowledgments

The authors thank Dr P Chaddah and Professor Ajay Gupta, for their support and encouragement, Mr P Saravanan, Mr M Gangrade, the staff of the low temperature and cryogenics laboratory for their technical support and Ms Deepti Jain for her interest. We acknowledge the support of DST, India for the LTHM Project and CSIR for a fellowship to SP. LSSC thanks Dr S B Roy, RRCAT, Indore for his encouragement.

## References

[1] Medvedev S *et al* 2009 *Nat. Mater.* **8** 630–3
[2] Hsu F C *et al* 2008 *Proc. Natl Acad. Sci. USA* **105** 14262
[3] Fang M H, Pham H M, Qian B, Liu T J, Vehstedt E K, Liu Y, Spinu L and Mao Z Q 2008 *Phys. Rev.* B **78** 224503
[4] Chen G F, Chen Z G, Dong J, Hu W Z, Li G, Zhang X D, Zheng P, Luo J L and Wang N L 2009 *Phys. Rev.* B **79** 140509
[5] Wu M K *et al* 2009 *Physica* C **469** 340
[6] Mizuguchi Y, Tomioka F, Tsuda S, Yamaguchi T and Takano Y 2009 *J. Phys. Soc. Japan* **78** 074712
[7] McQueen T M, Williams A J, Stephens P W, Tao J, Zhu Y, Ksenofontov V, Casper F, Felser C and Cava R J 2009 *Phys. Rev. Lett.* **103** 057002
[8] Janaki J, Geetha Kumary T, Mani A, Kalavathi S, Reddy G V R, Narasimha Rao G V and Bharthi A 2009 *J. Alloys Compounds* **486** 37–41
[9] Ge J, Cao S, Shen S, Yuan S, Kang B and Zhang J 2010 *Cryogenics* at press
[10] Ge J, Cao S, Shen S, Yuan S, Kang B and Zhang J 2010 *J. Appl. Phys.* **108** 053903
[11] Taen T, Tsychiya Y, Nakajima Y and Tamegai T 2009 *Phys. Rev.* B **80** 092502
[12] Millican J N, Phelan D, Thomas E L, Leao J B and Carpenter E 2009 *Solid State Commun.* **149** 707
[13] Williams A J, McQueen T M and Cava R J 2009 *Solid State Commun.* **149** 1507
[14] Ge M, Yand Z, Li L, Chen L, Pi L, Qu Z, Wang B, Sun Y and Zhang Y 2009 *Physica* C **469** 297–9
[15] Zhang S B, Lei H C, Zhu X D, Li G, Wang B S, Li L J, Zhu X B, Song W H, Yang Z R and Sun Y P 2009 *Physica* C **469** 1958–61
[16] Mok B H *et al* 2009 *Cryst. Growth Des.* **9** 3260–4
[17] Bhoi D, Sharath Chandra L S, Choudhury P, Ganesan V and Mandal P 2009 *Supercond. Sci. Technol.* **22** 095015
[18] Pandya S, Sherif S, Sharath Chandra L S and Ganesan V 2010 *Supercond. Sci. Technol.* **23** 075015
[19] Kaushik S D, Braccini V and Patnaik S 2008 *Pramana* **71** 1335–43
[20] Jaroszynski J *et al* 2008 *Phys. Rev.* B **78** 174523
[21] Thompson J R, Sorge K D, Cantoni C, Kerchner H R, Christen D K and Paranthaman M 2005 *Supercond. Sci. Tech.* **18** 970
[22] Jaroszynski J *et al* 2008 *Phys. Rev.* B **78** 064511
[23] Welp U, Xie R, Koshelev A E, Kwok W K, Cheng P, Fang L and Wen H-H 2008 *Phys. Rev* B **78** 140510 (R)
[24] Pallecchi I, Fanciulli C, Tropeano M, Palenzona A, Ferretti M, Malagoli A, Martinelli A, Sheikin I, Putti M and Ferdeghini C 2009 *Phys.Rev.* B **79** 104515
[25] Khasanov R *et al* 2008 *Phys. Rev.* B **78** 220510
[26] Palstra T T M, Batlogg B, Van Dover R B, Schneemeyer L F and Waszczak J V 1989 *Phys.Rev.* B **41** 6621
[27] Wang X L *et al* 2005 *J. Appl. Phys.* **97** 10B114
[28] Friedmann T A, Rice J P, Giapintzakis J and Ginsberg D M 1989 *Phys. Rev* B **39** 4258
[29] Abou-Aly A I, Awad R, Ibrahim I H and Abdeen W 2009 *Solid State Commun.* **149** 281–5
[30] Welp U, Fleshler S, Kwok W K, Klemm R A, Vinokur V M, Downey J, Veal B and Crabtree G W 1991 *Phys. Rev. Lett.* **67** 3180
[31] Kim D H, Gray K E and Trochet M D 1991 *Phys. Rev.* B **45** 10801
[32] Costa R M, Pureur P, Gusmao M, Senoussi S and Behnia K 2001 *Phys. Rev.* B **64** 214513